J Wood Sci (1998) 44:255–259
© The Japan Wood Research Society 1998

ORIGINAL ARTICLE

Takahisa Nakai · Kose Ando

Piezoelectric behavior of wood under combined compression and vibration stresses II: Effect of the deformation of cross-sectional wall of tracheids on changes in piezoelectric voltage in linear-elastic region*

Received: September 12, 1997 / Accepted: January 19, 1998

Abstract This study investigated and clarified the relation between the piezoelectric voltage and microscopic fracture of hinoki (*Chamaecyparis obtusa* Endl.), in particular the deformation of the cross-sectional wall of the tracheid in linear-elastic regions under combined compression and vibration stresses. The piezoelectric voltage–deformation (*P–D*) curve consisted of a linear region starting from the origin followed by a convex curved region. The linear region of the *P–D* curve was only about 60% of that of the load-displacement (*L–D*) curve. By applying combined stresses to a specimen, the cross-sectional walls of the tracheid were deformed mainly at the radial walls. When a tracheid was regarded approximately as a hexagonal prism, the elastic buckling stress of the radial wall was estimated from scanning electron microscope images and our method based on a modification of the Gibson and Ashby method. As a result, it was estimated that the elastic buckling stress was only about 80% of the stress at the proportional limit of the *P–D* curve. It is found that there are two consecutive regions before the proportional limit of the *P–D* curve: One is the region up to the spot where the radial cell wall generates the elastic buckling, and the other is the region starting from the end of the aforementioned region up to the proportional limit of the *P–D* curve.

Key words Piezoelectric voltage · Linear-elastic region · Elastic buckling stress

T · Nakai (✉)
Inititute of Wood Technology, Akita Prefectural College of Agriculture, Noshiro, 016-0876, Japan
Tel: +81-185-52-6987; Fax. +81-185-52-6976
e-mail: jaja@iwt.apca.ac.jp

K · Ando
School of Agricultural Science, Nagoya University, Nagoya 464-8601, Japan

*Part of this paper was presented at the 47th annual meeting of the Japan Wood Research Society, Kochi, April 3–5, 1997

Introduction

The purpose of this study was to clarify piezoelectric behavior during the deformation process of wood. In our previous paper[1] the relation between piezoelectric voltage and the deformation of tracheid in linear and nonlinear regions was reported mainly from the viewpoint of macroscopic phenomena observed with a scanning electron microscope (SEM). However, unsolved problems remain about the relation between the piezoelectric voltage and the microscopic structure of wood, as well as the generative mechanism of piezoelectric voltage in those regions. In this paper the behavior of the piezoelectric voltage in the linear-elastic region of the deformation process is investigated in detail.

Many attempts have been made over the years to model the shape of a wood cell. Young's modulus of a cell wall with the cell model has been calculated,[2–4] and the dynamic behavior has been studied by viewing the wood as a cellular solid.[5] However, the theoretical calculations of the amount of deformation are generally difficult, as a wood cell exhibits complicated deformation behavior and the constraints are complicated. A theoretical study of the dynamic behavior of cellular solids of metal and rubber has been performed and experimentally verified by Gibson and Ashby.[6] It is natural to attempt to calculate the amount of deformation at a cross-sectional wall of tracheid by applying the method of Gibson and Ashby to wood, which was successfully carried out in our study. Our method, which modified that of Gibson and Ashby, clarifies the deformation of a cross-sectional wall of a tracheid. Based on this result, the generative mechanism of the piezoelectric voltage in the linear-elastic region is elucidated.

Experiments

Specimens

The specimens used were made of kiln-dried hinoki (*Chamaecyparis obtusa* Endl.). The external form of the

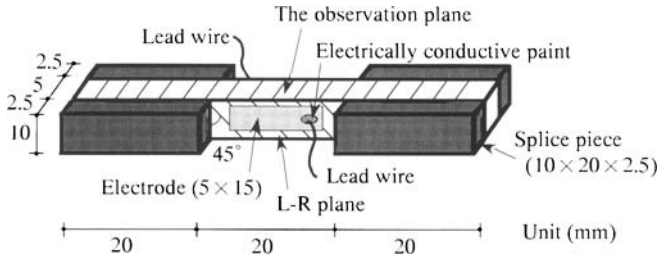

Fig. 1. Example of mounting a test specimen

specimen shown in Fig. 1 was 0.5 × 1 × 6 cm. Four splice pieces were attached to the specimen with adhesive to hold the specimen in the jig in the SEM chamber.

As shown in Fig. 1 we set the electrode plane on the L–R plane whose angle between the axial direction and the fiber direction of the specimen was 45°. As the electrode for detecting the piezoelectric voltage, platinum was spattered on the centers of the upper and lower surfaces of the specimen using a vacuum evaporator. The area of the electrode was 0.75 cm^2. Silver foil (thickness, length, width: 100 μm, 3 cm, 1 mm, respectively) was used as the lead wire. The piezoelectric voltage was detected by the measuring apparatus described previously.[1] The SEM observation plane of the specimen is shown in Fig. 1. Specimens were conditioned in a desiccator with P_2O_5 after vacuum-drying for 24 h.

The moisture contents of specimens were 5.5% and 3.3% immediately before the specimen was fixed to the jig in the chamber of the SEM and immediately after the observation, respectively. The averaged value of the specific gravity (ρ) of the specimens before observation was 0.43.

Loading method and measurement of piezoelectric voltage

The loading method and measurements of piezoelectric voltage were the same as in the previous study.[1]

Photography of specimens and image analysis

For analysis of the SEM image of the specimen during the deformation process, we used the software package NIH (National Institutes of Health) Image 1.56. This software was designed by Dr. Wayne Rasband.

Results and discussion

An example of a typical load-deformation (L–D) curve obtained from the combined compression and vibration test is shown in Fig. 2. At the beginning the load increases proportionally with displacement; then the L–D curve becomes convex, and there is a maximal point on the convex curve. The L–D curve then plateaus due to the buckling fracture of the specimen; finally, the load decreases suddenly with the shearing fracture in the 45° direction of the specimen. The piezoelectric behavior in the linear-elastic region of the first half of the L–D curve is investigated in detail in the piezoelectric voltage-deformation (P–D) curve as shown below.

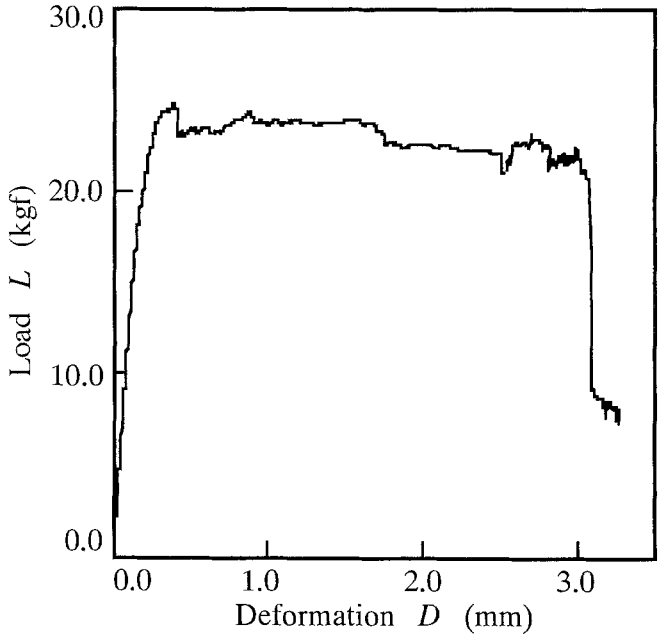

Fig. 2. Example of a load–deformation curve in the combined compression and vibration test

Relation between the proportional limit of the P–D and L–D curves

Parts of a P–D curve and an L–D curve are shown in Fig. 3. In this case the smoothing treatment was performed on the P–D curve to show it more clearly. At the beginning the P–D curve increases linearly and becomes convex, and it then decreases gradually after reaching a maximal point. The maximal point of the P–D curve coincides with the proportional limit of the L–D curve. Thus, after reaching the proportional limit of the L–D curve, the piezoelectric voltage decreased gradually. The L–D curve after the maximal point increases and shifts toward the plateau part caused by the buckling fracture of the specimen.

The regression analysis was done by regarding the linear part of the P–D curve as an approximately straight line. The proportional limit is defined as the point where the regression line, obtained from regression analysis for the linear part of the P–D curve, diverges from the P–D curve. Figure 4 was obtained by plotting the load ($L_{P\text{-}D}$) at the proportional limit of this curve for the load ($L_{L\text{-}D}$) and at the proportional limit of the L–D curve when the same treatment as mentioned above was done to the L–D curve. A linear relation holds between these parameters and can be approximated by the following equation

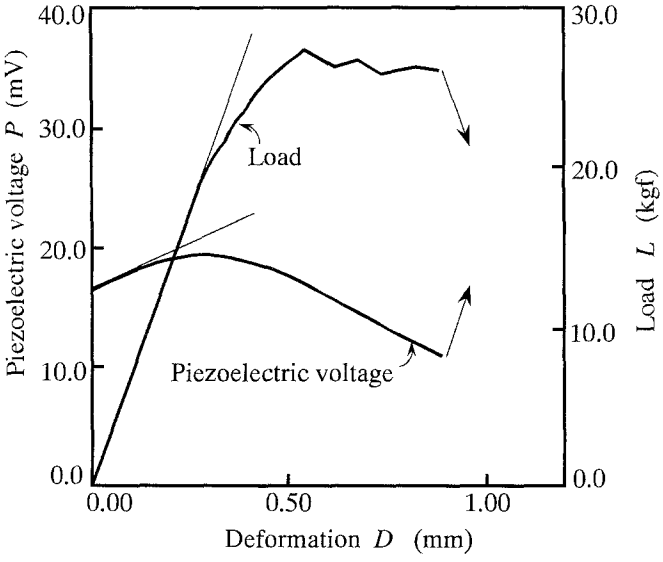

Fig. 3. Examples of piezoelectric voltage (P) and load (L) – deformation (D) curves. *Thin line*, regression line

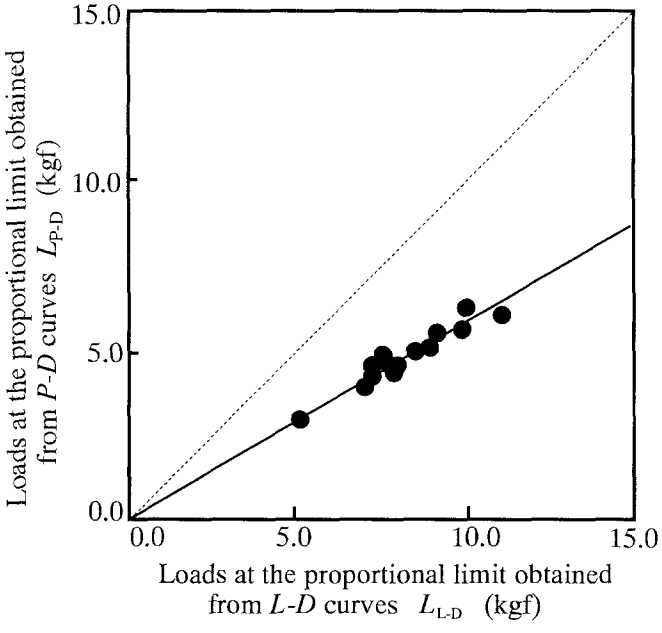

Fig. 4. Comparison of $L_{P\text{-}D}$ and $L_{L\text{-}D}$. *Solid line*, regression line, $L_{P\text{-}D} = 0.58 \times L_{L\text{-}D}$ ($R = 0.98$)

$$L_{P\text{-}D} = 0.58 \cdot L_{L\text{-}D} \tag{1}$$

From Eq. (1), it can be seen that the linear region of the P–D curve is only about 60% of that of the L–D curve. This result shows one of the most remarkable features of the P–D curve, but we must investigate more about the relation between the changes of P and deformation of the cell wall.

It is generally assumed that the piezoelectric effect of wood results from cellulose crystals. However, a natural cellulose cannot exist as a molecule in wood. A large number of cellulose molecular chains are composed of a fiber structure bundled with hemicellulose and lignin (i.e., a microfibril). A cell wall can be thought of as a framed structure of these microfibrils. Hence, it is presumed that the changing point from the linear to the nonlinear region of the P–D curve results from some gross deformations of the cell wall, generated by the shearing deformation among the cellulose molecular chains. In the next section, the state of deformation of a tracheid's wall is studied using SEM images.

Deformations of a cross-sectional wall of a tracheid and the resulting piezoelectric behavior

From the results of the SEM observation, the cross-sectional shape of the tracheid of specimen used in this study was predominantly hexagonal; a quadrangular shape was also observed slightly. Thus far, circular, quadrilateral, and hexagonal models have been proposed as cell models that show the cross-sectional shapes of tracheids. In this study, to make the analysis simple, we assumed that the cross-sectional shape of a tracheid is a hexagon, in agreement with the SEM images. Hence, a tracheid is regarded approximately as a hexagonal prism as shown in Fig. 5a, and the following analysis was used to calculate the elastic buckling stress of the cross-sectional wall of a tracheid. As shown in Fig. 5b, the plane with an angle of 45° against the cross section of the hexagonal prism as shown in Fig. 5a is visible in the SEM image. When the combined compression and vibration stresses (σ) was applied to a specimen, the cross-sectional wall of the tracheids deformed mainly at the radial walls, as shown in Fig. 5c. In this case, the radial wall was placed about in the 10th early wood from the boundary of the annual ring. Figure 5c is expressed in Fig. 5d. The pair of radial walls whose lengths are l_1 and l_2 are bent by σ. A magnified view of a wall deformed by σ is shown in Fig. 5e. From the equilibrium condition, the component of force acting on an area normal to the σ axis must be zero. On the other hand, the component of a force (P) acting on an area normal to the tangential axis is expressed by the following equation:

$$P = \frac{A}{2} \cdot \sigma = \left(h \cdot \cos\theta_3 + 2 \times l_1 \cdot \sin\theta_1\right) \cdot w \cdot \sigma \qquad \left(l_1 \cdot \sin\theta_1 = l_2 \cdot \sin\theta_2\right) \tag{2}$$

where A = the side area of the model as shown in Fig. 5b; l and h = the lengths of the radial and tangential walls, respectively; and t and w = the thickness and width of the wall, respectively. As shown in Fig. 5e, the normal force (P') applied to the radial wall is described by the following equation:

$$P' = \frac{P}{\cos\theta} \tag{3}$$

If the radial wall shown in Fig. 5e is viewed as a column with both ends fixed as shown in Fig. 5f, Euler's buckling stress P_{Euler} obtained using the elastic line method is defined by the formula

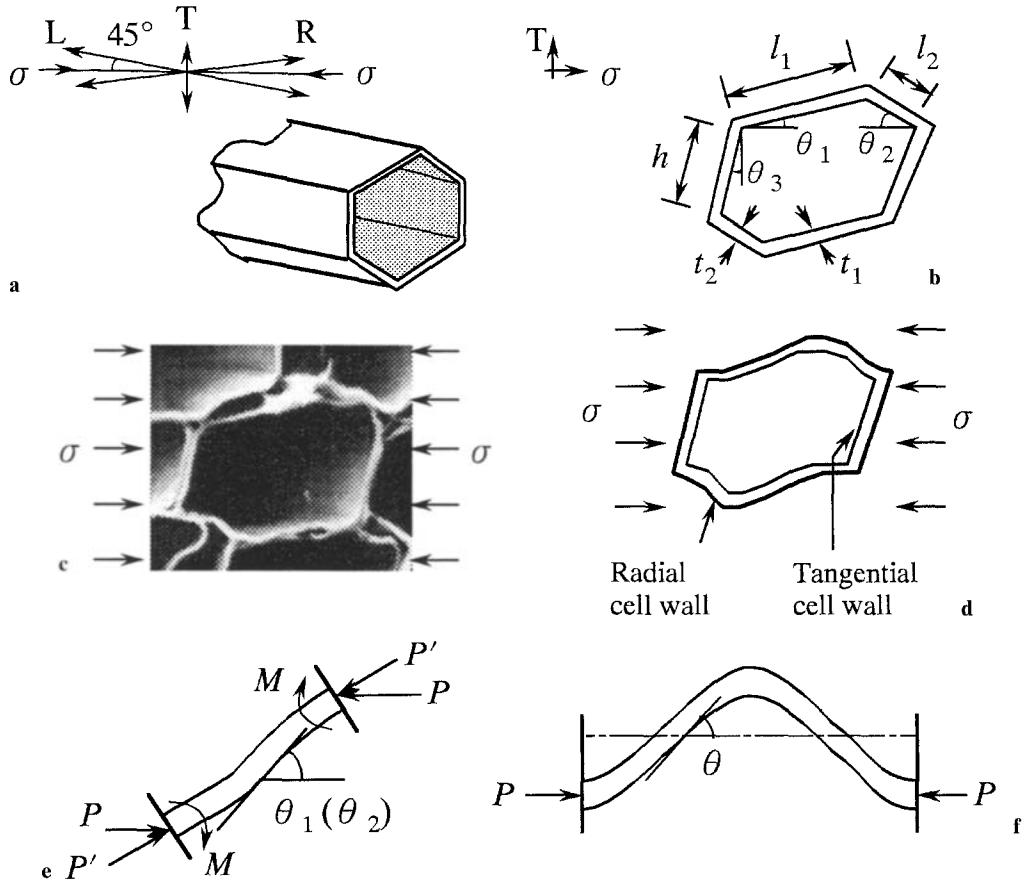

Fig. 5. Deformation of a cross-section of a tracheid. **a** Hexagonal model of a tracheid. **b** Cross section of a nondeformed tracheid. **c** Example of an scanning electron microscopic image of a cross section of a tracheid deformed after applying combined compression and vibration stresses (σ). **d** Model of a tracheid to which the combined compression and vibration stresses (σ) have been applied. **e** Model of a deformed radial wall. **f** Model of a piece of buckled column. l, h, length of the radial and tangential cell walls, respectively; t, thickness of the cell wall; P, compressive load; P', component force of P; M, bending moment; θ_1, θ_2, angle between the radial cell wall and the σ direction, θ_3, angle between the tangential cell wall and the T direction

$$P_{\text{Euler}} = \frac{n^2\pi^2 E_t I}{l^2} \tag{4}$$

Here, Young's modulus of a radial wall (E_t) is calculated from the following formula[2]

$$E_t \simeq \frac{E}{\rho^k} \simeq \frac{E}{1.50^{0.997}} \tag{5}$$

where k = a shape factor whose value was calculated by Ogama and Yamada[2] from Yamai's experimental results[7]; and E = Young's modulus of a specimen. The restrictional factor of the end, which provides a constraint condition between a cell and a neighboring cell (n), is given by the following formula[6]

$$n = \frac{2\psi^*}{\pi} \tag{6}$$

where ψ^* = the root of the following equation:

$$\tan\psi = \frac{2l}{h\psi} \tag{7}$$

That is,

$$\frac{2l}{h} = \psi\tan\psi \simeq \psi \cdot \frac{\psi - \frac{\psi^3}{3!} + \frac{\psi^5}{5!}}{1 - \frac{\psi^2}{2!} + \frac{\psi^4}{4!}} = \frac{120\psi^2 - 20\psi^4 + \psi^6}{120 - 60\psi^2 + 5\psi^4}$$

From these relations, we obtained the following equation for the elastic buckling stress $\sigma_{\text{cal.}}$.

$$\sigma_{\text{cal.}} = \frac{n^2\pi^2 t^3 \cos\theta_1}{12l_1^2(h\cos\theta_3 + 2l_1\sin\theta_1)} \cdot \frac{E}{1.50^{0.997}} \tag{8}$$

Figure 6 was obtained by plotting $\sigma_{\text{cal.}}$, calculated from Eq. (8) versus the proportional limit of the *P–D* curve. The experimental values of the cross-sectional shape of the tracheid measured with NIH Image (Table 1) were used in the above equation. A linear relation holds between these values and can be approximately given by the following equation:

$$\sigma_{cal.} = 0.83 \cdot \sigma_{P\text{–}D} \tag{9}$$

From Eqs. (1) and (9) it is observed that the radial wall of a tracheid generates elastic buckling at a point equal to half the value of the load at the proportional limit. As clarified from Eq. (9), it is estimated that the elastic buckling stress of a radial wall of a tracheid is only about 80% of the value of $\sigma_{P\text{–}D}$. From these results it is found that there are two consecutive regions before the proportional limit of the *P–D* curve: One is the region up to the spot where the radial cell wall generates the elastic buckling, and the other is the region starting from the end of the above region up to the proportional limit of the *P–D* curve. Hence, the *P–D* curve changed from the linear-elastic region to the convex-curved region as soon as a radial wall of the tracheid generated

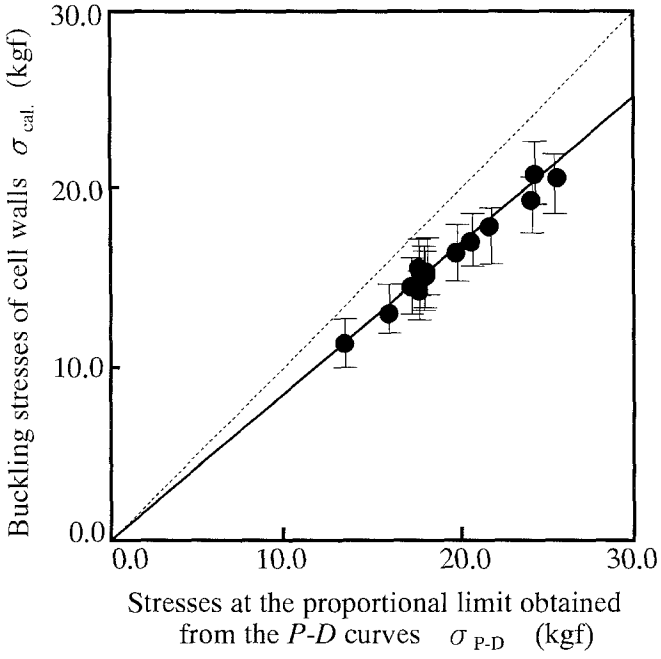

Fig. 6. Comparison of $\sigma_{cal.}$ (see Eq.8) and σ_{P-D} (proportional limit of the *P–D* curve). *Circles*, averaged value of one test specimen; *solid line*, regression line, $\sigma_{cal.} = 0.83 \times \sigma_{P-D}$ ($R = 0.97$). Upper and lower values of the standard deviation are shown by bars

Table 1. Measurements of the cross-section of tracheids

Measurement	Value
Length of radial cell wall (l) (μm)	
l_1	31.3–34.4
l_2	19.4–21.4
Length of tangential cell wall (h) (μm)	24.6–28.4
Thickness of cell wall t (μm)	
t_1	1.2–2.4
t_2	1.4–2.4
Angle (θ)(°)	
θ_1	8.7–14.0
θ_2	22.7–24.2
θ_3	14.0–15.3
Restrictional factor[a]	0.62–0.85

[a] Restrictional factor of the end, which provides a constraint condition between a cell and a neighboring cell.

elastic buckling. A maximal point on the convex curve was observed. The maximal point of the *P–D* curve coincides with the proportional limit of the *L–D* curve. After reaching the proportional limit of the *L–D* curve, the piezoelectric voltage decreased gradually. The *L–D* curve after the maximal point increased and shifted toward the plateau part caused by the buckling fracture of the specimen.

Analysis of the *P–D* curve beyond the proportional limit is beyond the scope of the present study. As reported in our previous paper,[1] a small uprush appears around the boundary of the annual ring and there is a clear peak of piezoelectric voltage at the shearing fracture in the 45° direction after the proportional limit; these generative mechanisms of piezoelectric voltage will be examined elsewhere.

Conclusion

This study investigated the relation between the piezoelectric voltage and microscopic fractures of hinoki (*Chamaecyparis obtusa* Endl.), in particular deformation of the cross-sectional wall of tracheids in linear-elastic regions under combined compression and vibration stresses. By applying these stresses to a specimen, the cross-sectional walls of tracheids were deformed mainly at the radial walls. The tracheid was regarded approximately as a hexagonal prism, and the elastic buckling stress of the cross-sectional wall of the tracheid was estimated from SEM images and our method, based on a modification of that of Gibson and Ashby. As a result, as soon as a radial wall buckled, the *P–D* curve changed from the linear-elastic region to the convex-curved region, and there was a maximal point on the convex curve. The maximal point of the *P–D* curve coincides with the proportional limit of the *L–D* curve. From these results, it can be concluded that the generative mechanism of piezoelectric voltage is related closely to the deformation (particularly to the elastic buckling) of cross-sectional walls of tracheids in the linear-elastic region. However, changes in the piezoelectric voltage after the proportional limit of the *P–D* curve still need to be investigated.

References

1. Nakai T, Naoyasu I, Kose A (1998) Piezoelectric behavior of wood under combined compression and vibration stresses: I. Relation between piezoelectric voltage and microscopic deformation of a sitka spruce (*Picea sitchensis* Carr.). J Wood Sci 44:28–34
2. Ogama T, Yamada T (1971) Porous structure of wood and its relaxation modulus (in Japanese). Zairyo 20:1194–1200
3. Ogama T, Yamada T (1974) Elastic modulus of porous material (in Japanese). Mokuzai Gakkaishi 20:166–171
4. Ogama T, Yamada T (1981) Young's moduli of earlywood and latewood in transverse direction of softwoods (in Japanese). Zairyo 30:707–711
5. Sawada M (1983) Elasticity and strength of wood as an anisotropic material (in Japanese). Zairyo 32:845–847
6. Gibson LJ, Ashby MF (1993) Cellular solids – Structure and properties. Cambridge University Press, Great Britain, pp 101–110
7. Yamai R (1955) Studies on the orthotropic properties of wood in compression (in Japanese). Ringyo Shikenjo Hokoku 113:69–70